Earth and Planetary Science Letters 619 (2023) 118311

Contents lists available at ScienceDirect

Earth and Planetary Science Letters

journal homepage: www.elsevier.com/locate/epsl

The deep Earth oxygen cycle: Mass balance considerations on the origin and evolution of mantle and surface oxidative reservoirs

Marc M. Hirschmann

Dept. of Earth and Environmental Sciences, University of Minnesota, Minneapolis, MN 55455 USA

ARTICLE INFO

Article history:
Received 8 March 2023
Received in revised form 7 July 2023
Accepted 8 July 2023
Available online xxxx
Editor: J. Badro

Keywords:
redox
oxygen fugacity
deep volatile cycles
deep Earth oxygen cycle

ABSTRACT

The deep Earth oxygen cycle addresses the origin and long-term exchange of oxidized species between the mantle and exosphere and creates the geochemical context in which the interior and surface environment have evolved. The redox power of the bulk silicate Earth (BSE) can be measured in terms of its redox budget, *RB*, relative to a reference state of the predominant valences of redox-sensitive elements in the mantle. 82±4% (1.9±0.5 × 10^{23} moles) of the redox power resides in the mantle and 18±4% (4.2±0.5 × 10^{22} moles) in the exosphere. Vigorous outfluxes of oxidized species from the mantle (3.8±0.7 × 10^{13} mol/yr) can replenish the exosphere reservoir in 1.1±0.2 Ga, which requires efficient long-term recycling of redox power via subduction. Within uncertainties, recent (last 200 Ma) mantle *RB* outfluxes and subduction influxes (4.9±1.3 × 10^{13} mol/yr) are balanced, but outfluxes likely exceeded influxes earlier in Earth history. CO_2 is 66±20% of the *RB* outfluxes but only 24±13% of the influxes. This is largely because of conjugate intervalence reactions; one in the shallow mantle creates carbonate at the expense of Fe_2O_3 and the other creates Fe_2O_3 from CO_2 on the surface by a combination of organic carbon fixation and oxidative weathering.

Scaling of mantle oxygen fugacity, f_{O2}, to redox mass balance is approximately $\Delta \log(^{Fe^{3+}}/_{Fe^{\top}})^{\text{peridotite}} \approx {}^{1}/_{4}\Delta \log(f_{O2})^{\text{mantle}}$. Consequently, inferences of secular evolution of mantle oxygen fugacity from the Archaean to the Proterozoic, amounting to about 1.5 log units in f_{O2}, imply that the Archaean mantle had an Fe^{3+}/Fe^{T} ratio <0.02, rather than the modern value of 0.04±0.01. Oceanic basalts derive from sources with greater redox budgets than mid-ocean ridges, and this is partly expressed as higher source Fe^{3+}/Fe^{T} ratios, but more importantly, as greater source CO_2 concentrations. In combination, these require that plumes in the deep upper mantle have Fe^{3+}/Fe^{T} ratios significantly greater than the depleted mantle.

The oxidative inventory of the BSE originated by a combination of H_2O disproportionation in the atmosphere, leading to H_2 escape, and FeO disproportionation in the deep mantle, with loss of Fe to the core. FeO disproportionation in a deep magma ocean inevitably produces a significant fraction of the BSE *RB*, but additional contributions are likely required. Further Fe loss could be from bridgemanite crystallization followed by Fe escape through a basal magma ocean. Gradual mixing of the resulting deep oxidized layer may account for secular oxidation of the mantle source regions of igneous rocks from 3 to 2 Ga. H_2O disproportionation assisted in accumulation of the oxidized surface species, but was not a significant source of mantle oxidative power, as mechanisms of oxidative influx are quantitatively insufficient.

1. Introduction

Earth's oxidized surface and interior reservoirs are essential features of its chemical geodynamics. In the exosphere (the crust, surface, and fluid envelopes), abundant oxidized species, Fe_2O_3, carbonate, sulfate, and dioxygen, are salient features of Earth's geology, climate, and biogeochemistry. In the mantle, oxidized iron and carbon affect geophysical properties, the locus of melting, and fluxes of redox power between the interior and the surface. In many respects, the reservoirs and fluxes of oxidative power between the interior and surface are analogous to Earth's deep volatile cycles, which are key to the maintenance of equable surface conditions and are coupled to the geodynamics and geochemistry of the solid planet (Dasgupta and Hirschmann, 2010; Korenaga et al., 2017). Therefore, the origin and evolution of Earth's oxidative reservoirs constitute a deep Earth oxygen cycle.

The redox evolution of Earth's exosphere is a critical feature of the planet's history, as exemplified by the multi-stage rise of at-

E-mail address: mmh@umn.edu.

https://doi.org/10.1016/j.epsl.2023.118311

mospheric dioxygen (Lyons et al., 2014). The advent of dioxygen was preceded and accompanied by accumulation of much larger reservoirs of condensed oxidized species (carbonate, Fe_2O_3, sulfate) in rocks and sediments (Hayes and Waldbauer, 2006). The formation of the oxidized Fe-C-S surface reservoirs has been attributed to volcanogenic fluxes originating in the mantle (Kasting et al., 1993; Holland, 2002; Kump and Barley, 2007; Gaillard et al., 2011; Kadoya et al., 2020), and/or selective return of reduced material via subduction (Hayes and Waldbauer, 2006), or by loss of H_2 to space (Catling et al., 2001; Kasting, 2013; Zahnle et al., 2019). If the oxidized surface derived from a net flux of oxidants from the interior, the mantle should have become correspondingly reduced. Yet, evidence from mantle-derived rocks has found either negligible temporal change (Canil, 1997; Delano, 2001) or evidence for secular oxidation with time (Aulbach and Stagno, 2016; Nicklas et al., 2018, 2019; Stagno and Aulbach, 2022). The opposite has also been considered, that the mantle has become oxidized by return of surface material (Lecuyer and Ricard, 1999; Kump et al., 2001; Evans, 2012), and surface-derived oxidants are evident in recycled sources of oceanic island basalts (OIB) (Moussallam et al., 2019). Mutual oxidation of the surface and interior, or oxidation of the surface with constant mantle redox power, are seemingly inconsistent with closed system behavior for the combined reservoirs and would require net external redox fluxes, either by hydrogen escape to space or supply of oxidized material from the deep Earth (Andrault et al., 2018; Nicklas et al., 2019; O'Neill and Aulbach, 2022; Stagno and Aulbach, 2022). Alternatively, they may reflect closed-system changes in mantle oxygen fugacity (f_{O2}) owing to secular decreases in mantle temperature or changing conditions in the source regions of mantle-derived magmas (Gaillard et al., 2015; Gaetani, 2016).

As is also true for deep planetary volatile cycles, essential aspects of the deep Earth oxygen cycle are the processes and circumstances by which the bulk silicate Earth (BSE) acquired its inventory of oxidative power. The silicate portions of terrestrial planets originated in the presence of plentiful Fe-rich alloy, as evidenced by the metal content of primitive meteorites and by the planets' large metallic cores. Earth is not the sole terrestrial planet with an oxidized surface, but it is the only one known to have appreciable ferric iron in its mantle, which potentially represents a much larger reservoir. The high net oxidation state of the bulk silicate Earth could have originated by H_2O disproportionation, leading to H_2 escape (Kasting et al., 1993; Catling et al., 2001; Zahnle et al., 2019), and by FeO disproportionation, either associated with bridgmanite crystallization in the lower mantle (Frost et al., 2004) or in a deep magma ocean (Hirschmann, 2012; Armstrong et al., 2019; Hirschmann, 2022).

Evaluation of the deep Earth oxygen cycle demands quantification of the net fluxes of oxidized species between the surface and interior reservoirs. Accrual of the oxidized surface reservoir at the expense of the mantle requires extended periods in which oxidized outfluxes exceeded influxes. In contrast, oxidation of the mantle by import of oxidants produced by atmospheric H_2 escape (Zahnle et al., 2019) requires sustained periods of greater influx. Compared to many such studies focused on deep Earth volatile cycles, deep redox fluxes have received less attention. Biogeochemical mass balance treatments examining redox fluxes between lithosphere and fluid envelopes (e.g., Hayes and Waldbauer, 2006; Stolper et al., 2021) do not account for all fluxes to and from the mantle. Evans (2012) evaluated the detailed redox influxes to the mantle at modern subduction zones and also summed redox outfluxes at ridges and oceanic islands. Also, Brounce et al. (2019) conducted a redox mass balance focused on the Marianas subduction zone. Evans (2012) concluded that modern influxes exceed outfluxes, implying net oxidation of the mantle. Both influxes and outfluxes merit reevaluation, especially in light of new constraints on volatile fluxes averaged over the last 200 Ma of tectonic history (Wong et al., 2019).

Exosphere redox dynamics are generally appraised in terms of mass balance, quantifying net oxidant/reductant fluxes and accumulations (Berner, 2003; Hayes and Waldbauer, 2006). Mantle redox is more typically quantified with f_{O2} (Cottrell et al., 2021; Stagno and Aulbach, 2022), which doesn't provide direct information about mass balance. Therefore, relating coupled redox mantle-exosphere evolution and dynamics requires scaling between mantle f_{O2} and redox mass balance. For example, this is needed to calculate the change in *RB* corresponding to inferred shifts in mantle f_{O2} from the Archaean to the present (Aulbach and Stagno, 2016; Nicklas et al., 2019). Such scaling has been calculated previously (Parkinson and Arculus, 1999; Evans, 2012; Luth and Stachel, 2014), but not applied to evidence for secular redox evolution of the mantle.

The goals of this paper are to evaluate the mass balances and fluxes underpinning Earth's deep oxygen cycle and the origin of Earth's oxidized redox budget. The specific coupling between the solid Earth and atmospheric oxygen (see Kasting, 2013; Stolper et al., 2021) is not addressed directly here. Rather, the aim is to better illuminate the large-scale context in which redox evolution has occurred.

2. Reference states and redox budgets

2.1. Reference state redox budget

In quantifying redox mass balances, it is necessary to establish a reference valence state for each redox-sensitive element (Evans, 2012; Kasting, 2013). For the deep Earth oxygen cycle, the principal elements of interest are Fe, S, C, Cr, and H, and the reference valence states are those that predominate in the upper mantle: Fe^{2+}, S^{2-}, C^0, Cr^{3+}, and H^+. An important distinction between the treatment here and some studies focused on surficial oxidative reservoirs is that C^{4+}, as carbonate or CO_2, is considered to be an oxidized species (Hayes and Waldbauer, 2006; Evans, 2012) because the predominant state of C in the mantle is neutral C (Stagno et al., 2013).

To quantify the redox mass balances of the mantle and exosphere, we adopt the Redox Budget (*RB*) formalism of Evans (2012), where the *RB* is given in moles of electrons required to bring the mass back to the reference state:

$$RB = \sum_i n_i V_i, \tag{1}$$

where n_i is the number of moles of a species i in a reservoir and v_i is the number of electrons required to take one atom of species i to its reference state. *RB*, positive for materials more oxidized than the reference state and negative for those more reduced, is an extensive quantity, applicable to reservoirs and fluxes. It is also useful to consider the redox budget per unit mass of rock, m,

$$\overline{RB} = \frac{\sum_i n_i V_i}{m} \tag{2}$$

with units of moles/gram.

2.2. Exosphere oxidized budget

Appreciable oxidized species in the exosphere include dioxygen, sulfate and pyrite, carbonate, and ferric iron. The net exosphere *RB* is $4.2\pm0.5 \times 10^{22}$ moles. Atmospheric O_2 accounts for only 0.4% of the exosphere *RB*, whereas carbonate accounts for 71.4%, crustal Fe_2O_3 24.6%, and sulfate and pyrite combined 3.6% (Table 1, Fig. 1).

Table 1
Redox Budget (*RB*) of the exosphere.

	RB factor* *moles /mole*	Species *X 10^{18}* moles	*RB*	% of total
Exosphere				
CO_2[a]	4	7510±1280	30,000±5100	71.4
Fe_2O_3[b]	2	5170±965	10,300±1930	24.6
SO_3[c]	8	166±50	1330±400	3.2
FeS_2[c]	2	90±27	179±54	0.4
O_2[d]	4	37	148	0.4
Sum			**42,040±5470**	
Mantle *(see Supplement for sources)*				
Fe_2O_3	2	90000±25000	180,000±50,000	95.7
CO_2	4	600±100	-[e]	
Sulfide	0.4	27500±2500	11000±1000	5.9
CrO	−1	−3000±3000	−3000±3000	−1.6
Sum			**190,000±50,000**	

* number of electrons per molecule relative to reference state for species.
[a] Hirschmann (2018). Note that organic carbon, with approximate stoichiometry of CH_2O, is redox-neutral compared to the assumed reference state.
[b] Lecuyer and Ricard (1999).
[c] Rickard (2014).
[d] Stolper et al. (2021).
[e] The contribution of CO_2 to mantle is incorporated into the Fe_2O_3 value (see Supplement).

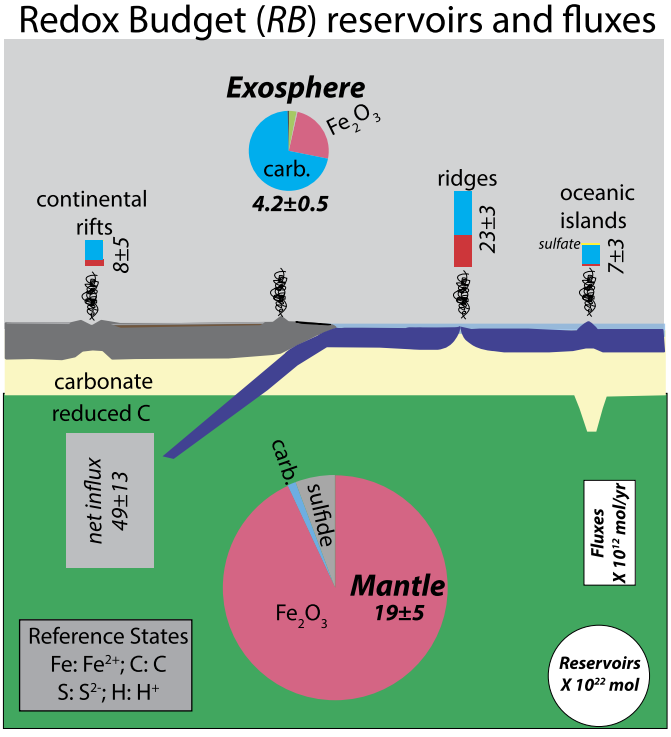

Fig. 1. Redox budget (*RB*) reservoirs and fluxes for the recent (~200 Ma) deep Earth oxygen cycle. Values are in moles of electrons relative to the reference oxidation states of the elements (see text and Evans, 2012). Exosphere and mantle reservoir *RB* values from Table 1 and fluxes from Tables 2 and 3. The net influx at subduction zones is the sum of fluxes into the mantle after taking into account the return of oxidants to the surface environment from volcanic and non-volcanic arc fluxes (Evans, 2012). Reservoirs and outfluxes are color-coded by chemical species, but minor contributions (e.g., atmospheric O_2, pyrite, sulfate, CrO) are not necessarily illustrated or labeled.

2.3. Mantle redox reservoir

Although there is redox heterogeneity in the mantle (Cottrell et al., 2021; Stagno and Aulbach, 2022), the initial assumption here, revisited in Section 4.7, is that it is not vertically stratified and therefore that the whole mantle *RB* can be characterized from observations in the upper mantle. The well-known decrease in f_{O2} with depth, caused by pressure-dependent changes in intermineral partitioning of Fe^{3+} (Frost and McCammon, 2008), and ferrous iron disproportionation to Fe^0 and Fe_2O_3 (Frost et al., 2004) occurs at constant $\overline{RB}$, i.e., the $\overline{RB}$ is equal on either side of the reaction

$$3FeO \rightleftharpoons Fe_2O_3 + Fe. \quad (3)$$

The *RB* of the consequential redox-sensitive elements in the mantle, Fe, C, S, and Cr, are tabulated in Table 1, with additional details in the Supplement. Iron is nearly entirely Fe^{2+} (~96±1%; see Supplement). The majority of carbon in the mantle is neutral, occurring as diamond, carbide, or dissolved in sulfide liquid (Stagno et al., 2013; Zhang et al., 2019), but there is a small shallow portion of the uppermost mantle in which carbonate is stable. Sulfur occurs as sulfide liquid (Zhang et al., 2019) with an effective valence close to S^{2-}, but allowing for non-stoichiometric M/S ratios in real oxysulfide liquids makes a small contribution to upper mantle *RB*. Cr occurs almost entirely as Cr^{3+} (>96%; Hirschmann, 2022), and hydrogen is assumed to occur solely as H^+ (i.e., H_2O or OH^-). The total *RB* of the mantle amounts to 1.9±0.5 × 10^{23} moles (Table 1) and the $\overline{RB}$ is 5 × 10^{-5} mol/g, with 95.7% coming from Fe_2O_3, 5.9% from oxysulfide liquid, and −1.6% from Cr^{2+}.

Table 2
Redox Budget (*RB*) outfluxes from mantle.

	Ridges	Oceanic Islands	Continental	Sum	% of total
Volume (km^3)	23.9±2.3	1.1±0.2	2.5±1.8		
	Species fluxes × 10^{12} mol/yr				
Fe_2O_3	5.0±0.7	0.5±0.1	1±0.7	6.5±1	
CO_2	3.3±0.7	1.5±0.6	1.5±1.2	6.3±1.5	
SO_4^{2-}	-	0.01	0.002	0.01	
	RB fluxes × 10^{12} mol/yr				
Fe_2O_3	10±1.4	0.9±0.2	2±1.5	13±2	34
CO_2	13±3	6±3	6±5	25±6	65.7
SO_4^{2-}	-	0.09	0.02	0.1	0.3
Sum	**23±3**	**7±3**	**8±5**	**38±7**	
% of total	61	18	21		

All values from this work, as described in the main text and Supplement.

2.4. Redox outfluxes and influxes

Outfluxes of oxidants from the mantle, summarized in Table 2 and Fig. 1, include Fe_2O_3, CO_2, and SO_4^{2-} dissolved as magmatic species, from ridges, oceanic islands, and intracontinental provinces. Fluxes from arcs are best considered as a factor in the inefficient return of oxidants to the mantle via subduction (Evans, 2012). Averaged over the last 200 Ma, magmatic production at ridges and intracontinental sources, 23.9±2.3 and 2.5±1.7 km^3/yr, as well as the rate of oxidant influxes at subduction zones, are greater than modern rates (Wong et al., 2019), as detailed in the Supplement. For oceanic islands, the magmatic volume flux, 1.1±0.2 km^3/yr, is calculated from well-studied inputs in Hawaii (Lipman and Calvert, 2013) and scaled globally based on the fraction (21%) of buoyancy flux that Hawaii contributes to the global total (King and Adam, 2014).

2.4.1. Redox outfluxes

Redox outfluxes are given in Table 2 and described in the Supplement. Here we briefly highlight the fluxes of CO_2 from oceanic islands and continental rifts, though further details of these estimates are also in the Supplement.

On the basis of CO_2/He ratios, Marty and Tolstikhin (1998) calculated an upper limit for the oceanic island CO_2 flux of ≤3.3 ×

Table 3
Subduction Influxes.

	C^{4+}	Fe^{3+}	other[a]	Sum
	RB Fluxes $\times 10^{12}$ *mol/yr*			
Sediments	4.8±2.4[b]	1.5±0.3[c]	0.9±0.1[c]	7.2±2.5
AOC	8.2±1.2[b]	16.6±8.1[c]	7.4±0.4[c]	32.2±8.2
Serp	5.3±3.2[b]	9.7±7.6[c]	4.6±.6[c]	19.7±8.3
Arc	−6.3±−3.7[b]	-6.0±2.9[c]	−2.7±.6[c]	−15.0±5.1
non-volcanic fluids	−0.3±0.23[c]	-	5.3±4.1[c]	5.0±4.1
Sum	**11.8±5.7**	**21.8±11.5**	**15.6±4.2**	**49.1±13.4**

[a] other=*RB* fluxes from S, H, and non-carbonate C.
[b] Carbonate or CO_2 fluxes averaged over the last 200 Ma from Wong et al. (2019).
[c] modern fluxes of Fe, S, H, and non-carbonate C from Evans (2012), multiplied by a factor of 1.45 to take into account greater average rates of subduction (strike length X orthogonal convergence rate) over the last 200 Ma from Wong et al. (2019). Fluxes from Evans (2012) are taken from the midpoints of given "maximum" and "minimum" assessments.

10^{12} mol/yr. In contrast, Wong et al. (2019) estimated a flux of 0.5±0.25 × 10^{12} mol/yr CO_2 from a compilation of OIB localities for which published data were available, though they warned that this was an incomplete survey of worldwide sources. Hauri et al. (2019) estimated a total OIB flux of 0.17-0.35 × 10^{12} mol/yr by combining melt inclusion CO_2/Ba and CO_2/Rb ratios with total intraplate basalt and Ba fluxes derived from seamount ocean bathymetry. Unfortunately, this approach omits both intrusive magmatic inputs and the limiting effects of isostasy on the expression of total magmatic output for oceanic islands and large seamounts. The new estimate, 1.5±0.6 × 10^{12} mol/yr (Table 2) also uses CO_2/Ba ratios, but constrains Ba outfluxes from a survey of OIB, weighted by hotspot buoyancy fluxes (Table S1).

It has been recognized recently that passive, non-volcanic degassing at rifts is a large fraction of global CO_2 outflux, possibly exceeding that at ridges by a factor of 2-3. (Brune et al., 2017; Wong et al., 2019). This corresponds to *RB* fluxes over the last 200 Ma as great as 2.5 × 10^{13} mol/yr, or potentially about half the global outflux. However, the estimates are dominated by high CO_2 outgassing observed in the East African rift and Italy, which may not apply to the global 26,000 km array of rifts. We favor a conservative approach, proposed by Brune et al. (2017), with smaller estimated overall fluxes (6 × 10^{12} mol/yr; Table 2).

2.4.2. Subduction influxes

Treatment of subduction redox fluxes begins with the survey of modern rates from Evans (2012). We consider the total subduction *RB* influx as the difference between the incoming subducted lithosphere minus fluxes returned to the surface via arcs and metamorphic belts, and this approach is not affected by redox depletion that can occur by deep convection of mantle wedges (Brounce et al., 2019). Here we update, including net deep CO_2 fluxes over the last 200 Ma from Wong et al. (2019), (*RB* influx=1.2±0.6 × 10^{13} mol/yr Table 3). No similar time-dependent constraints are available for other redox carriers (other forms of C, Fe, S, H). For these we take the means of maximum and medium modern rates cataloged by Evans (2012), and multiply them by 1.45 (3.7±1.2 × 10^{13} mol/yr Table 3), the factor between the subduction rate averaged over the last 200 Ma and the modern rate (Wong et al., 2019).

2.5. Total RB reservoirs and fluxes

The total BSE (=mantle+exosphere) *RB* is 2.3±0.5 × 10^{23} moles, of which 82±4% is in the mantle and 18±4% in the exosphere. The total *RB* flux from the mantle to the exosphere is 3.8±0.7 × 10^{13} mol/yr (Table 2), which is greater than estimated by Evans (2012) (2.3±0.6 × 10^{13} mol/yr), who adopted a smaller CO_2 flux from ridges and did not incorporate continental sources. CO_2 accounts for 66% of the *RB* outflux, Fe_2O_3 for 34%, and SO_4^{2-}

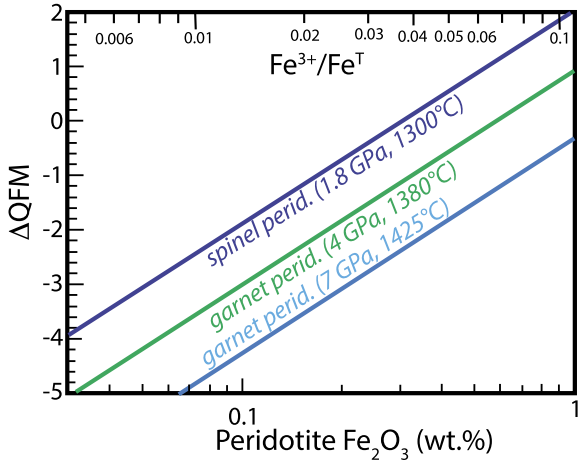

Fig. 2. Calculated oxygen fugacity (log f_{O2}) relative to the QFM buffer for garnet and spinel peridotite as a function of bulk peridotite Fe_2O_3 content and Fe^{3+}/Fe^T ratio. For spinel and garnet peridotite, calculations at indicated conditions are conducted using the oxybarometers of Wood and Virgo (1989) and Stagno et al. (2013), with further details in the Supplement. Fe_2O_3 contents of garnet and spinel as a function of bulk peridotite composition are calculated from inter-mineral partition coefficients, as detailed in the Supplement. Absolute values of ΔQFM diminish with increasing pressure, but at any fixed conditions, the log-log slopes are all close to 0.25.

less than 1%. 61% of the *RB* flux comes from ridges, 18% from oceanic islands, and 21% from intracontinental regions. The net *RB* influx at subduction zones averaged over the last 200 Ma is 4.9±1.3 × 10^{13} mol/yr, consisting of 44±22% Fe_2O_3, 24±13% carbonate, and the balance from S, H, and non-carbonate C species. It is similar to the modern rate (4.6±1.2 × 10^{13} mol/yr) appraised by Evans (2012), owing to a smaller contribution from subducting carbonate and a correspondingly greater influx of Fe_2O_3

3. Relationship between f_{O2} and mantle Fe_2O_3

To relate the mantle redox budget with variations in mantle f_{O2}, we present calculations for fertile lherzolite in spinel peridotite and garnet peridotite facies mantle. Calculations are based on spinel and garnet oxybarometers (Wood and Virgo, 1989; Stagno et al., 2013) combined with inter-mineral partition coefficients and peridotite mineral modes, as detailed in the Supplementary Information. Calculated values of f_{O2} in units of ΔQFM (=logarithmic difference from the quartz-fayalite-magnetite buffer) depend logarithmically on Fe^{3+}/Fe^T and therefore on bulk peridotite Fe_2O_3 (Fig. 2). Though volume effects induce more reduced conditions relative to QFM with increased pressure, spinel and garnet peridotite display composition-f_{O2} slopes in log-log space that are near-constant and similar to 0.25, as all mineral and melt iron redox buffers have a simplified stoichiometry of

$$FeO + 1/4O_2 \rightleftharpoons FeO_{1.5} \quad (4)$$

(O'Neill et al., 1993). Therefore, for each log unit change in f_{O2}, the Fe^{3+}/Fe^T ratio (approximately similar to the Fe^{3+}/Fe^{2+} ratio when Fe^{3+} concentrations are small) changes by a factor of ~1.8 ($10^{1/4}$).

$$\Delta \log(Fe^{3+}/Fe^{\top})^{\text{peridotite}} \approx 1/4 \Delta \log(f_{O2})^{\text{mantle}} \quad (5)$$

The significant consequence is that at reduced conditions (low total Fe_2O_3), small changes in Fe_2O_3 contents produce large effects on ΔQFM, and at more oxidized conditions, shifts in ΔQFM are commensurately smaller.

4. Discussion

4.1. Photosynthesis and the development of the exosphere RB

Readers are likely to note that photosynthesis and the great oxygenation event are not emphasized in this work. Though essential to the rise of high P_{O2} of Earth's surface, in the context of development of the exosphere *RB* reservoir, photosynthesis plays no direct role. This is partly because the photosynthetic reaction

$$CO_2 + H_2O = CH_2O + O_2 \quad (6)$$

is neutral with respect *RB*, as it transfers +4 electrons/mole *RB* from CO_2 to O_2. More generally, chemical reactions occurring within the exosphere cannot modify the exosphere *RB* without subsequent fluxes of either oxidized or reduced reaction products to the interior or to space. A common paradigm is that photosynthesis produces an oxidized surface when coupled to burial (i.e., subduction) of organic carbon (Berner, 2003; Hayes and Waldbauer, 2006; Stolper et al., 2021). However, CH_2O is neutral with respect to *RB* in the mantle reference state, as it has the same *RB* as C + H_2O. Therefore, in Reaction 6, it is the original supply of CO_2 that provides the positive exosphere *RB* and formation of the exosphere reservoir of CO_2 is the essential prerequisite for photosynthetic development of high P_{O2} on the surface. The processes of interest in the present work are those that produced and maintained a positive *RB* reservoir (CO_2 + Fe_2O_3) in Earth's exosphere.

4.2. Fluxes

The estimated *RB* mantle outflux, 3.8±0.7 × 10^{13} mol/yr, is sufficient to accrue the entire exosphere *RB* in 1.1±0.2 Ga. The combination of short exosphere replenishment time and predominance of the mantle *RB* reservoir (Fig. 1) is consistent with significant recycling of *RB* to the mantle, as is also true for the deep carbon cycle (Hirschmann, 2018), highlighting the strong coupling between the two. Combining the outflux of 3.8±0.7 × 10^{13} mol/yr with the recent deep subduction *RB* flux, 4.9±1.3 × 10^{13} mol/yr, yields a net influx of 1.1±1.5 × 10^{13} mol/yr, apparently smaller than that, 2.3±1.3 × 10^{13} mol/yr, surmised by Evans (2012). Thus, within uncertainty, either modern outfluxes and influxes are nearly balanced or influxes could be modestly greater than outfluxes.

CO_2 dominates the *RB* outflux (66±20%), but makes a lesser contribution to the influx (24±13%). This is owing partly to complementary intervalence reactions between C and Fe creating carbonate during upwelling to the shallow mantle

$$\underset{\text{reduced}}{C} + 2\underset{\text{silicate}}{Fe_2O_3} \rightleftharpoons \underset{\text{carbonate}}{CO_2} + 4\ \underset{\text{silicate}}{FeO}, \quad (7)$$

and the net reaction combining organic carbon fixation (Reaction 6) and oxidative weathering on the surface

$$\underset{\text{vapor}}{CO_2} + 4\ \underset{\text{silicate}}{FeO} + H_2O \rightleftharpoons \underset{\text{organic C}}{CH_2O} + 2\underset{\text{silicate}}{Fe_2O_3}. \quad (8)$$

Reaction (7) is intimately associated with melting in the upper mantle, with important geophysical and geochemical consequences (Hirschmann, 2010; Stagno et al., 2013), whereas reaction (8) is foundational to the biogeochemical carbon cycle (Hayes and Waldbauer, 2006). Surficial formation of sulfate and mantle reduction to sulfide contribute additional intervalence coupling to the deep oxygen cycle.

Considering the long-term history of redox exchange, *RB* influxes may have been smaller in proportion to outfluxes during earlier periods of Earth history. Fe_2O_3 and CO_2 outfluxes scale with global magmatic production, which was greater on an earlier hotter Earth, as do CO_2 influxes via subduction, which are controlled mostly by plate spreading rates (Sleep and Zahnle, 2001). However, the largest single modern influx of *RB*, Fe_2O_3 in altered oceanic crust (Table 3), was significantly smaller before the Phanerozoic, when oceans lacked oxygenated bottom water (Stolper and Keller, 2018). Therefore, lower net influxes of Fe_2O_3 prevailed in the Neoproterozoic. In the Archaean and Paleoproterozoic (3.8-1.7 Ga; Johnson and Molnar, 2019), banded iron formations (BIF) could have contributed significant *RB* influxes. Thompson et al. (2019) evaluated the Archean carbon-iron cycle associated with BIF formation and estimated methane production at 2.5 Ga of 3.2 ± 2.5 × 10^{12} mols/yr, which produces enough Fe_2O_3 to support an *RB* influx of 1.3±1.0 × 10^{13} mols/yr, about the same as recent Fe_2O_3 influxes in altered oceanic crust. In summary, though the magnitude of net *RB* exchange between the surface and interior through Earth history remains uncertain, net influxes previous to the Phanerozoic were either smaller than or similar to present rates. Relevant to the discussion below, there is no evidence or identified mechanism to infer extended periods where net influxes greatly exceeded present-day values.

Notably, S does not contribute significantly to mantle oxidant outfluxes. Great emphasis has been placed on a possible shift from volcanogenic H_2S to SO_2 from mantle-derived magmas, and its effect on atmospheric oxidation (Holland, 2002; Kump and Barley, 2007; Gaillard et al., 2011; Kadoya et al., 2020). However, the sulfur emanating from the mantle has always been dominated by S^{2-} (Section 2.3). A shift from venting of SO_2 as compared to H_2S, as may occur owing to degassing of subareal and hotter magmas rather than submarine or cooler volcanism (Kump and Barley, 2007; Gaillard et al., 2011; Kadoya et al., 2020), occurs in crustal magma chambers or volcanic conduits, as SO_2 is produced at the expense of Fe_2O_3:

$$\underset{\text{magma}}{FeS} + 3\underset{\text{magma}}{Fe_2O_3} \rightleftharpoons \underset{\text{vapor}}{SO_2} + 7\ \underset{\text{magma}}{FeO}, \quad (9)$$

(Brounce et al., 2017). This provides an oxidant that is more readily available to biogeochemical cycles, favoring atmospheric or ocean oxidation, but does not influence directly the redox mass balance of the surface reservoir.

4.3. Origin of bulk silicate Earth RB inventory

The Earth accreted from materials rich in metal, and silicate equilibrated with metal at low pressure would have had negligible *RB*. The net oxidizing power of the BSE was produced by some combination of FeO and H_2O disproportionation (Fig. 3). H_2O disproportionation proceeds according to reaction (3) and

$$\underset{\text{vapor}}{2H_2O} \rightleftharpoons 2\ \underset{\text{vapor}}{H_2} + \underset{\text{vapor}}{O_2} \quad (10)$$

(Hamano et al., 2013; Pahlevan et al., 2019; Zahnle et al., 2019), or equivalently

$$\underset{\text{vapor}}{H_2O} + 2\ \underset{\text{silicate}}{FeO} \rightleftharpoons \underset{\text{vapor}}{H_2} + \underset{\text{vapor}}{Fe_2O_3}. \quad (11)$$

FeO disproportionation occurs at high pressure, either in a deep magma ocean (Hirschmann, 2012, 2022; Armstrong et al., 2019), or from bridgmanite crystallization (Frost et al., 2004) and increases mantle *RB* if the alloy is removed to the core. Disproportionation of H_2O could have occurred in early reducing atmospheres from the time of the magma ocean (Hamano et al., 2013) to as recently as the Paleoproterozoic (Zahnle et al., 2019) and increases BSE *RB* when atmospheric H_2 escapes to space (Fig. 3).

Based on the equation of state of Deng et al. (2020), Hirschmann (2022) found that FeO disproportionation in a deep magma ocean can produce Fe^{3+}/Fe^{T} ratios of 0.03-0.1 for reasonable estimates of

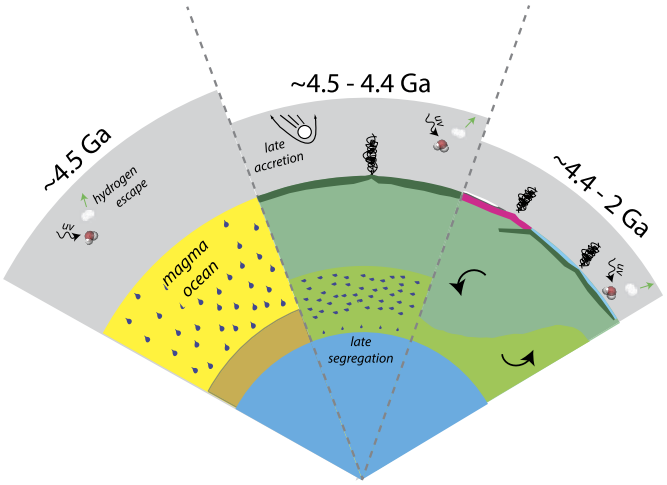

Fig. 3. Origin and evolution of Earth's Redox Budget (*RB*). (A) During the magma ocean stage at ~4.5 Ga, Fe_2O_3 is produced by FeO disproportionation in a deep magma ocean, as silicate and core-destined alloy interact. Magma ocean degassing potentially forms a thick CO_2-rich atmosphere. Also, H_2O disproportionation followed by H_2 escape increases the oxidation state at the surface. (B) Between ~4.5 and 4.4 Ga, crystallization of the magma ocean leads to precipitation of alloy (and bridgmanite) in the lower mantle. A portion of the alloy segregates to the core, possibly by sinking through a basal magma ocean, forming a lower mantle region that is enriched in Fe_2O_3. The basal magma ocean may persist past 4.4 Ga. Late accretion of metalliferous planetesimals adds significant reduced material, neutralizing much of the oxidized budget of the surface and near-surface. Impactors also ablate the thick post-magma-ocean atmosphere. Volcanogenic outfluxes contribute to mantle-exosphere *RB* exchange. Influxes of oxidants (carbonate) or reductants (accreted alloy) to the mantle are also likely, but not shown in diagram. (C) After cessation of significant late accretion, from 4.4 to ~2 Ga, evolution of the *RB* occurs owing to continued H_2O disproportionation and loss of H_2 to space and to gradual convective mixing of the deep mantle oxidized layer with the shallower mantle. Together with H_2 escape, volcanogenic outfluxes build the surface *RB* inventory, which is stored in sediments and in the crust. Tectonic processes also recycle oxidants back to the mantle.

core-forming conditions, but that these are diminished by ~0.04 by subsequent oxidation of CrO to Cr_2O_3 during crystallization, which diminishes mantle *RB* by $\sim 1.5 \times 10^{23}$ moles. Therefore, FeO disproportionation in a magma ocean had the potential to supply to the early-solidified mantle Fe_2O_3 comparable to the present-day value ($Fe^{3+}/Fe^{T} = 0.04 \pm 0.01$) only if core formation occurred at high temperature (>4000 K) (Hirschmann, 2022). If core-forming conditions were not so extreme, or if significant reductants were added to the mantle during post-magma ocean late-accretion (see section 4.4), additional sources of mantle *RB* were required from either bridgmanite crystallization or H_2 escape.

A recent experimental study (Kuwahara et al., 2023) suggests that disproportionation of the terrestrial magma ocean produced a mantle with an Fe^{3+}/Fe^{T} ratio of 0.35±0.15, which corresponds to a BSE *RB* of $1.6 \pm 0.7 \times 10^{24}$ moles, or 4-10 times greater than is observed at present. This is far greater than the plausible negative *RB* contributed by Cr oxidation or added by late accretion ($-0.2 \pm 0.1 \times 10^{24}$ moles, see section 4.4 below). If accurate, the results of Kuwahara et al. (2023) represent a profound challenge to present understanding of the evolution of mantle redox mass balance.

Previous work has placed different emphasis on the relative roles of iron versus H_2O disproportionation in the overall net oxidation state of the Earth (Kasting et al., 1993; Catling et al., 2001; Armstrong et al., 2019; Pahlevan et al., 2019; Zahnle et al., 2019; Sossi et al., 2020; Hirschmann, 2022). During the magma ocean stage, H_2 escape from a steam atmosphere could produce a maximum mantle *RB* of 3.5×10^{22} moles (Hamano et al., 2013), less than 20% of the present-day BSE value. To supply the rest of the present-day mantle *RB* by subsequent downward penetration of H_2O-disproportionated oxidant, as advocated by Zahnle et al. (2019), would require large influx rates. The mantle appears to have reached its present-day *RB* inventory at about 2 Ga (Stagno and Aulbach, 2022), and so supply of oxidant from the surface to the interior in the previous 2.5 Ga would require a net influx of $\sim 1 \times 10^{14}$ mols/yr, about 4-10 times greater than the recent net influx value ($1.1 \pm 1.5 \times 10^{13}$ mol/y). As noted in section 4.3, there is no evidence or known mechanism for such enhanced ancient influxes, and so H_2O disproportionation was subordinate to FeO disproportionation in the accrual of the interior *RB* reservoir.

Following magma ocean solidification, lower mantle crystallization drove FeO disproportionation that produced additional Fe_2O_3. The very great stability of Fe^{3+} in bridgmanite exceeds that in silicate melt at any given temperature, pressure, and f_{O2}; i.e. the minimum Fe^{3+}/Fe^{T} of crystalline "pyrolite" at 25 GPa and 1973 K at metal saturation is >0.2 (Huang et al., 2021) whereas a silicate liquid at similar conditions has a ratio no greater than 0.04 (Hirschmann, 2022). Consequently, bridgmanite precipitation from the cooling magma ocean forced additional Fe_2O_3 production and alloy precipitation. This buffered the Fe_2O_3 content of the crystallizing magma, which invalidates models that treat Fe_2O_3 as a compatible or incompatible species during lower mantle differentiation (Maurice et al., 2023). Removal of a small amount of the alloy to the core can account for much of the BSE not produced in the magma ocean. For example, removal of metal amounting to 0.1 wt.% of the mantle mass would enhance the BSE *RB* by 1.4×10^{23}, or about 3/4 of the present-day value.

4.4. Early surface RB reservoir and late accretion

The redox conditions of the Earth's early surface, after the dramatic events of Earth's differentiation, degassing, and solidification, have long been debated, with particular emphasis on the relationship between redox conditions, early climate, and the potential for prebiotic chemistry (Miller and Urey, 1959; Walker, 1977; Catling and Zahnle, 2020). Two competing contributions are development of a thick oxidized atmosphere descended from a magma ocean (Hirschmann, 2012; Armstrong et al., 2019; Sossi et al., 2020) and production of a reduced surface from addition of a "late veneer" after the last giant impact (Schaefer and Fegley, 2010; Pahlevan et al., 2019; Zahnle et al., 2020; Itcovitz et al., 2022) (Fig. 3). A massive magma ocean atmosphere with a CO_2 pressure of 10 MPa, possibly abetted by graphite precipitation on cooling (Sossi et al., 2020), would amount to an *RB* ($\sim 5 \times 10^{22}$ moles), similar in magnitude to the modern surface *RB* reservoir, but most would be ablated by impacts (Schlichting et al., 2015; Sinclair et al., 2020) or removed by weathering and early rapid recycling (Sleep and Zahnle, 2001). On the other hand, late-accreted material was likely derived from the inner solar system and metal rich (Hopp et al., 2020; Zahnle et al., 2020; Itcovitz et al., 2022). If late accreted bodies totaled 0.7±0.2 wt.% of the BSE mass (Jacobson et al., 2014) and averaged 20±10% metal, similar to enstatite chondrites, this could add an *RB* of $-2.1 \pm 1.2 \times 10^{23}$ moles, a quantity comparable in magnitude but of opposite sign to the present-day BSE *RB*. The proportions of this material delivered directly to the surface and mantle depended on the size distribution of impactors, but the larger magnitude *RB* of the late accreted material as compared to a potential thick CO_2-atmosphere indicates that the early surface reservoir *RB* was negative and therefore reduced (Zahnle et al., 2020).

The destruction of a negative *RB* surface reservoir occurred from a combination of H_2 escape, oxidized fluxes from the interior, and burial of the early protocrust by subsequent magmatism. The latter, aided by impacts (Borgeat and Tackley, 2022), could have contributed a flux of reductants to the interior. We know from platinum group element concentrations and isotopes that late accreted

material was eventually transferred to the mantle (Maier et al., 2009; Creech et al., 2017; Fischer-Gödde et al., 2020), but whether much of its reductive power was first neutralized on the surface is more difficult to gauge. If significant Fe alloy was transferred to the mantle, the large remaining positive *RB* of the modern mantle suggests that the early mantle had yet more abundant oxidizing power.

4.5. Secular evolution of the surface and the mantle

In the aftermath of late accretion, the surface *RB* reservoir was negligible or possibly negative and so it has grown through geologic time by a combination of fluxes from the mantle and H_2 loss to space. At the same time, evolution of the mantle *RB* reservoir can be considered.

If the surface reservoir became oxidized entirely owing to H_2O disproportionation and H_2 escape, then the total H_2O lost would have been equivalent to approximately 1/4 exospheres (1 exosphere H_2O=1.6 $\times$ 10^{21} grams, Hirschmann and Dasgupta, 2009). Depending on continental area, this amounts to 700-1000 meters reduction in continental freeboard from the beginning of the Hadean to the Paleoproterozoic, when the more oxidized atmosphere terminated effective H_2 escape (Zahnle et al., 2019), or less if some portion of the H_2O was supplied from the mantle. The corresponding amount of H_2 escaped to space is equivalent to 8 modern atmospheres (800 kPa), which is well within the limits given by D/H ratios and fractionation of Xe isotopes by hydrodynamic escape (Pahlevan et al., 2019; Zahnle et al., 2019).

Though the accrual of the surface *RB* chiefly from H_2 escape is plausible, it is likely that a significant fraction derived from the interior because nearly 3/4 of the modern surface *RB* is in the form of carbonate (Fig. 1), which accumulated from volcanogenic outgassing of CO_2 (Hayes and Waldbauer, 2006). Evidence that the mantle was about 1.5 log units more reduced in the Archaean (Aulbach and Stagno, 2016; Nicklas et al., 2018, 2019) does not change this inference, as under those mildly reducing conditions, the predominant carbonic gas would also have been CO_2 (Gaillard et al., 2022).

Alternatively, if the entire present-day surface *RB* came from the mantle, then the mantle Fe_2O_3 concentration has diminished by 0.09 wt.% since the early Hadean; i.e., a Hadean Fe^{3+}/Fe^{T} ratio of 0.05±0.01 compared to 0.04±0.01 today. This would correspond to approximately 0.4 log units of secular decrease in mantle f_{O2} (Fig. 2). No such trend is evident in mantle redox proxies, though its small magnitude may not be resolvable. It seems likely that the oxidized surface *RB* mass comes from a combination of interior fluxes and H_2 escape, and that any record of reduction of the mantle owing to *RB* outfluxes is small and overwhelmed by other effects.

Early work (Canil, 1997; Delano, 2001; Trail et al., 2011) detected no measurable change in mantle f_{O2} since the early Hadean. More recently, studies of olivine/bulk rock V partitioning of picrites and komatiites (Nicklas et al., 2018, 2019) and of V/Sc and Fe^{3+}/Fe^{T} ratios in eclogites and ophiolitic basalts (Aulbach and Stagno, 2016; Aulbach et al., 2019) indicate that mantle f_{O2} has increased by ~1.5 log units since the Archaean, with most of the change happening between 3.5 and 2 Ga (Fig. 4). Although V-based oxybarometers may not be uniquely attributable to differences in mantle f_{O2} (Laubier et al., 2014; Cottrell et al., 2021), we consider the ramifications if the inferred secular mantle oxidation occurred. The alternative hypothesis, that mantle f_{O2} has been near constant, is discussed further in the Supplementary Information.

Evidence for secular increases in f_{O2} is apparent both in plate margin basaltic lithologies, derived from the upper mantle, and komatiites, sourced from the lower mantle (McKenzie, 2020). Therefore, inferred temporal f_{O2} shifts apply to a significant mantle

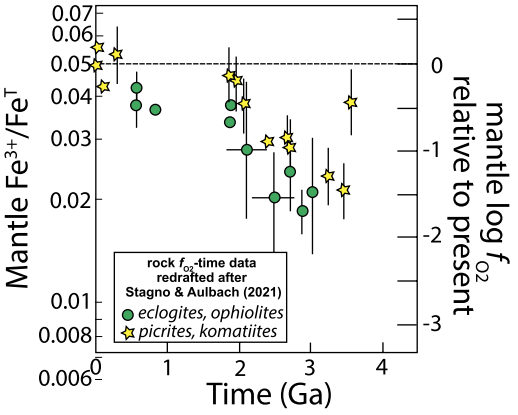

Fig. 4. Secular change in mantle f_{O2} and corresponding Fe^{3+}/Fe^{T} through geologic time. Oxygen fugacities, from V/Sc and Fe^{3+}/Fe^{T} ratios recorded in komatiitic and basaltic rocks, are relative to values recorded in recent picrites, with data compiled by Stagno and Aulbach (2022). The scale on the right side of the diagram indicates the value of log f_{O2} relative to that recorded by V/Sc ratios for modern mantle, assuming that the latter correspond to a mantle Fe^{3+}/Fe^{T} of 0.04, as indicated on the left side of the diagram. Mantle Fe^{3+}/Fe^{T} ratios are the corresponding ratios calculated from the slope shown in Fig. 2 relative to the assumed modern value of 0.04. The approximately 1.5 log unit f_{O2} change since the Archaean indicates mantle source regions for komatiitic and basaltic magmas with Fe^{3+}/Fe^{T} less than 0.02.

mass fraction. Relative to the modern mantle with an assumed Fe^{3+}/Fe^{T} ratio of 0.04±0.01, the paleooxybarometers imply that the mantle at 3 Ga had an Fe^{3+}/Fe^{T} ratio of <0.02 (Fig. 4). Therefore, a ~1.5 log unit f_{O2} change through the Archaean/Proterozoic transition (Fig. 4) could require that the early Archaean mantle had less than half of its present-day *RB* and that half of the $\overline{RB}$ in magma source regions was gained since.

It is generally considered that the mantle approached comparatively oxidizing conditions, a "great mantle oxidation event" (Scaillet and Gaillard, 2011), in the early Hadean and then either experienced little subsequent change (e.g., Trail et al., 2011) or experienced comparatively small changes in the intervening 4.4 Ga (Aulbach and Stagno, 2016; Nicklas et al., 2018, 2019). This view, justified from the point of view of f_{O2}, may be inaccurate in terms of *RB*. Rather, the significant oxidation relative to cosmochemical precursors, evident from the earliest Hadean mantle may have required only small amounts of *RB*, and the modest changes in f_{O2} in the subsequent 4 Ga (if verified), suggest increases in mantle *RB* of equal or perhaps greater magnitude.

Taken at face value, the large change in mantle *RB* that corresponds to the apparent secular increase in f_{O2} (Fig. 4) requires mixing of an appreciable mass of oxidized material into the source regions of mafic and ultramafic magmas from the Archaean to the Paleoproterozoic. If together these sources represent the majority of the mantle mass, then as noted in section 4.2, it is doubtful that this magnitude change could derive from surface influx. Therefore, if the increases in mantle redox inferred from ancient basalts and komatiites are accurate, an internal source, such as gradual mixing of a deep oxidized layer originating in the lower mantle by iron disproportionation (Andrault et al., 2018; O'Neill and Aulbach, 2022) is more probable (Fig. 3). The required time scale for this mixing is similar to that suggested by the gradual mantle homogenization of ^{142}Nd isotopic anomalies evident in Archaean but not younger rocks (Hyung and Jacobsen, 2020).

Mass balance considerations of a deep oxidized layer can be evaluated from the following scenario. Assume that the earliest solidified mantle had an Fe^{3+}/Fe^{T} of 0.02 (Fig. 4) and that the oxidized surface reservoir at this time was negligible. In the lower mantle, this bulk composition was expressed as a combination of minerals with a net Fe^{3+}/Fe^{T} ratio >0.02 and some fraction of disproportionated Fe alloy. According to the thermodynamic model of

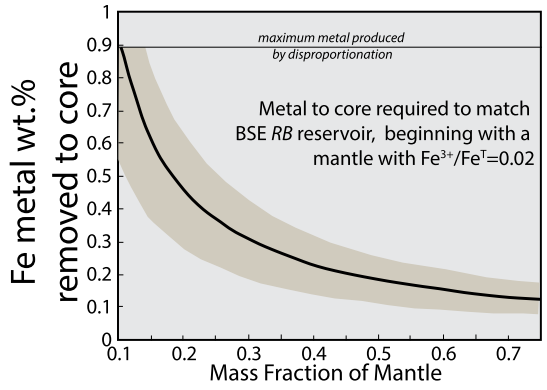

Fig. 5. Model calculation showing the fraction of Fe alloy that would have to be lost to the core from a lower mantle layer of a given mass, relative to the whole-mantle mass, in order to account for the total BSE *RB*. The alloy would be formed by disproportionation during bridgmanite crystallization. The calculation assumes that prior to this loss of alloy, the bulk mantle Fe^{3+}/Fe^{T} ratio was 0.02, and that afterwards, it is 0.04±0.01. At a ratio of 0.02, the lower mantle consists of bridgmanite, ferropericlase, and 0.09% alloy. For a thin layer, all of this metal would need to drain to the core. If loss occurred throughout the lower mantle (0.75 mass of the mantle), then the required fraction of alloy lost would be 0.12%.

Huang et al. (2021), this alloy fraction would be ∼0.9 wt.%. Complete loss of this alloy to the core throughout the lower mantle would have produced a BSE *RB* of 1.3 × 10^{24} moles, more than 5 times the present value. Therefore, loss had to be partial, consistent with the conclusion that the present-day lower mantle today contains ∼0.6 wt.% alloy (Huang et al., 2021). Partial loss of the alloy to the core would produce an oxidized mantle layer that through convective mixing, enhanced Fe^{3+}/Fe^{T} in the upper mantle and ultimately supplied the *RB* of the oxidized surface reservoir (O'Neill and Aulbach, 2022). The fraction of necessary alloy loss depends on the thickness of the deep layer that experienced metal extraction (Fig. 5). For example, if the layer comprised the lower 50% (by mass) of the mantle, then 0.18±0.07 wt.% alloy, ∼1/4 of that available in the layer, was lost to the core. Alternatively, for near-total metal extraction the layer would have had to been limited to about 10% of the mass of the mantle, or a layer above the CMB ∼500 km thick.

This exercise demonstrates that secular mantle redox evolution could have arisen from an oxidized deep layer created by export of disproportionated alloy to the core, provided that the scope of alloy loss was limited. The mechanism that allowed only a small portion of lower mantle alloy to escape to the core is unknown, but could have been a permeability threshold for metallic liquid. Alternatively, during solidification of a basal magma ocean, alloy coprecipitating with bridgmanite may have sunk to the core (Fig. 3). More complex scenarios are also feasible, as the earliest solidified mantle may have been redox stratified, owing either to the effects of late accretion (Zahnle et al., 2020), making shallow regions more reduced, or magma ocean fractional crystallization in the upper mantle (Maurice et al., 2023), making them more oxidized.

4.6. Secular variation in mantle temperature and redox

Petrologic evidence indicates that the mantle cooled by ∼200 degrees over the last 3 Ga (Herzberg et al., 2010), and this potentially could change the f_{O2} of mantle-derived basalt relative to standard (e.g., QFM) buffers without any open system change in *RB*. For example, Gaetani (2016) found that the f_{O2} imposed by a spinel peridotite source becomes more oxidized for cooler mantle potential temperatures and Gaillard et al. (2015) suggested that shallower melting accompanied a cooler mantle should correspond to more oxidized conditions, owing to the well-known effect of pressure on f_{O2} in garnet peridotite (e.g., Frost and McCammon, 2008). However, other factors also are relevant. For example, at constant bulk rock Fe^{3+}/Fe^{T}, garnet peridotite enforces more oxidizing conditions compared to spinel peridotite (Stolper et al., 2020), and so diminishing contributions from garnet peridotite relative to spinel peridotite would have an influence opposite to the oxidizing effect of cooling for spinel peridotite alone. Therefore, Fe_2O_3 could be less compatible in garnet peridotite residua than spinel peridotite, and consequently, for a source with a given $\overline{RB}$, the Fe_2O_3 released from deeper melting may be greater than the shallower melting of a cooler mantle. The quantitative effects of mantle cooling on release of oxidants to the surface, including effects on the release of carbonate, need further experimental and thermodynamic investigation.

4.7. Redox heterogeneity in the mantle

As is true for most geochemical parameters, different mantle domains record heterogeneities in f_{O2}, and therefore in $\overline{RB}$. Apart from well-established f_{O2} diversity associated with convergent margins and continental lithosphere (Cottrell et al., 2021), studies of oceanic basalts reveal systematic differences between MORB and OIB in Fe^{3+}/Fe^{T} ratios (Brounce et al., 2017, 2022; Hartley et al., 2017; Moussallam et al., 2019) and CO_2 contents (Marty and Tolstikhin, 1998; Hirschmann, 2018), implying that OIB source regions also have greater $\overline{RB}$.

Fe^{3+}/Fe^{T} ratios of OIB range from slightly lower than MORB (0.14±0.02; Zhang et al., 2018) up to nearly 3 times greater (Brounce et al., 2017, 2022; Hartley et al., 2017; Moussallam et al., 2019). This suggests Fe_2O_3 enrichments in OIB source regions, but is also partly owing to melting effects, as Fe_2O_3 enrichments are enhanced at smaller degrees of partial melting and at higher pressure. For example, thermodynamic calculations indicate that Fe_2O_3 of incipient partial melts of garnet peridotite at 3.5 GPa is twice as great as for spinel peridotite at 1.2 GPa, though this difference diminishes with increasing melt fraction (Jennings and Holland, 2015). For OIB with Fe^{3+}/Fe^{T} ratios of 0.2±0.05, typical of OIB localities with high extents of partial melting such as Hawaii and Iceland (Brounce et al., 2017; Hartley et al., 2017), source regions may have Fe^{3+}/Fe^{T} ratios between 0.04 and 0.06, or 100-150% of the MORB source. More compositionally extreme OIB generated by smaller extents of melting such as from the Canary Islands or Erebus, with Fe^{3+}/Fe^{T} ratios of 0.3-0.35 (Moussallam et al., 2019) likely require source ratios of 0.06-0.08.

CO_2 is a relatively minor component of the $\overline{RB}$ in MORB sources, but contributes significantly in OIB sources, which have total $\overline{RB}$ of between 7.5-15 × 10^{-5} mol/g, compared to MORB, with 4-6 × 10^{-5} mol/g (Fig. 6). Therefore, in the deep upper mantle beneath OIB sources, where carbon is reduced and Fe_2O_3 enhanced according to the reverse of reaction (7) (Stagno et al., 2013; Moussallam et al., 2019), approximate Fe^{3+}/Fe^{T} ratios range from 0.06-0.07 (Réunion) up to 0.09-0.13 (Canaries) (Fig. 6). Compared to background mantle with Fe^{3+}/Fe^{T} near 0.04 and negligible C, these deep sources have f_{O2} between 0.75 and 2 log units more oxidized (Fig. 6). At shallower depths, the conversion of this reduced carbon to carbonate decreases the available Fe_2O_3 and consequently partially buffers log f_{O2} in OIB source regions.

The Canary Islands source has strong geochemical signatures of recycled oceanic lithosphere (Taracsák et al., 2019), and so it is not surprising that it is also markedly oxidized relative to typical depleted upper mantle. Geochemical markers of recycling in Hawaii and Iceland are less pronounced and their sources sample relatively primitive ^{3}He-enriched domains. Perhaps such domains are also more oxidized than the depleted upper mantle, potentially because they contain deep mantle remnants enhanced by bridgmanite disproportionation.

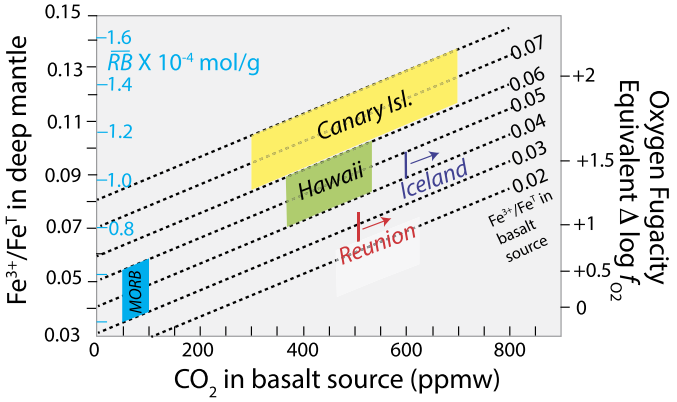

Fig. 6. Relationship between basalt source region Fe^{3+}/Fe^{T} ratios (dashed isopleths) and CO_2 concentrations and total $\overline{RB}$ in the mantle source at depth, where carbon is in reduced form rather than as carbonate (e.g., Stagno et al., 2013). In the deep mantle, the *RB* is expressed as an enhanced Fe^{3+}/Fe^{T} ratio, owing to interconversion of Fe and C oxidation states ($CO_2 + 4FeO = 2\ Fe_2O_3 + C$). The prevailing oxygen fugacity, relative to a reference mantle at the same depth but with Fe^{3+}/Fe^{T} =0.04 and zero CO_2, is enhanced according to the relationship shown in Fig. 2. For oceanic islands, source $\overline{RB}$ includes contributions from inferred Fe^{3+}/Fe^{T} of the sources, estimated from ratios measured in erupted glasses (Brounce et al., 2017; Hartley et al., 2017; Moussallam et al., 2019; Brounce et al., 2022) and source CO_2 concentrations. The latter for Hawaii and Canary Islands are from Tucker et al. (2019) and Taracsák et al. (2019). For Iceland and Réunion, minimum source CO_2 concentrations are taken from the maximal value inferred from the nearest plume-affected ridge segment (Hauri et al., 2019). MORB source CO_2 is from Rosenthal et al. (2015).

Oceanic Island basalts are thought to sample an enriched portion of the lower mantle amounting to approximately 20% of the BSE mass (Arevalo et al., 2013). If this region has an average $\overline{RB}$ of 1×10^{-4} mol/g, then the *RB* of the mantle and BSE have been underestimated by about 20%.

5. Conclusions

Deep planetary geochemical cycles entail large scale exchange of components between the surface and interior, together with key effects of the exchanged components on surface and interior dynamics. In this respect, planetary-scale redox fluxes constitute a deep Earth oxygen cycle.

82±4% of Earth's redox budget, *RB*, resides in the mantle, and 18±4% in the exosphere. Vigorous exchange between surface and interior reservoirs involves chiefly outfluxes oxidize carbon and influxes of oxidized iron and carbon. Iron is oxidized on the surface from CO_2 by a combination of photosynthesis and oxidative weathering; carbon is oxidized in the interior from Fe_2O_3 by redox melting.

Evidence for secular evolution of mantle oxygen fugacity from ~3 Ga to ~2 Ga implies doubling of the $\overline{RB}$ of basalt source regions over that time interval, probably owing to gradual mixing of deep oxidized mantle that originated by bridgmanite disproportionation.

The oxidized character of the BSE arose owing to a combination of FeO disproportionation in the deep mantle and H_2O disproportionation in the atmosphere, though the latter likely affected the surface more than the interior. FeO disproportionation in a deep magma ocean produced a significant fraction of the modern *RB*, but additional contributions from bridgmanite disproportionation and subsequent loss of metal to the core were likely also essential.

The deep sources of mantle plumes carry a significantly greater $\overline{RB}$ than the upper depleted mantle, and much of this signal is transmitted as enriched CO_2 in OIB source regions.

CRediT authorship contribution statement

Marc M. Hirschmann: Writing – review & editing, Writing – original draft, Methodology, Funding acquisition, Formal analysis, Conceptualization.

Declaration of competing interest

The authors declare that they have no known competing financial interests or personal relationships that could have appeared to influence the work reported in this paper.

Data availability

all data used are in manuscript, tables, or supplement

Acknowledgements

This work benefitted from conversations and email exchanges with Dan Frost, Kaveh Pahlevan, Terry Plank, Tony Withers, and Tamsin Mather, from helpful reviews by Sonja Aulbach and Maryjo Brounce, and from guidance from the editor, James Badro. Many thanks to Suzanne Birner for sharing her Jupyter notebook for spinel oxybarometry and Rong Huang for consultation about her lower mantle f_{O2} calculator. I am grateful for support from the National Science Foundation though grant EAR2016215. This work was completed during a stay at the Bayrisches Geoinstitut enabled by a fellowship from the Alexander von Humboldt Sitftung.

Appendix A. Supplementary material

Supplementary material related to this article can be found online at https://doi.org/10.1016/j.epsl.2023.118311.

References

Andrault, D., Muñoz, M., Pesce, G., Cerantola, V., Chumakov, A., Kantor, I., Pascarelli, S., Rüffer, R., Hennet, L., 2018. Large oxygen excess in the primitive mantle could be the source of the great oxygenation event. Geochem. Perspect. Lett. 6, 5–10.
Arevalo, R., McDonough, W.F., Stracke, A., Willbold, M., Ireland, T.J., Walker, R.J., 2013. Simplified mantle architecture and distribution of radiogenic power. Geochem. Geophys. Geosyst. 14, 2265–2285.
Armstrong, K., Frost, D.J., McCammon, C.A., Rubie, D.C., Ballaran, T.B., 2019. Deep magma ocean formation set the oxidation state of Earth's mantle. Science 365, 903–906.
Aulbach, S., Stagno, V., 2016. Evidence for a reducing Archean ambient mantle and its effects on the carbon cycle. Geology 44, 751–754.
Aulbach, S., Woodland, A.B., Stern, R.A., Vasilyev, P., Heaman, L.M., Viljoen, K.S., 2019. Evidence for a dominantly reducing Archaean ambient mantle from two redox proxies, and low oxygen fugacity of deeply subducted oceanic crust. Sci. Rep. 9.
Berner, R.A., 2003. The long-term carbon cycle, fossil fuels and atmospheric composition. Nature 426, 323–326.
Borgeat, X., Tackley, P.J., 2022. Hadean/Eoarchean tectonics and mantle mixing induced by impacts: a three-dimensional study. Prog. Earth Planet. Sci. 9, 1–19.
Brounce, M., Cottrell, E., Kelley, K.A., 2019. The redox budget of the Mariana subduction zone. Earth Planet. Sci. Lett. 528, 115859.
Brounce, M., Stolper, E., Eiler, J., 2017. Redox variations in Mauna Kea lavas, the oxygen fugacity of the Hawaiian plume, and the role of volcanic gases in Earth's oxygenation. Proc. Natl. Acad. Sci. USA 114, 8997–9002.
Brounce, M., Stolper, E., Eiler, J., 2022. The mantle source of basalts from Reunion Island is not more oxidized than the MORB source mantle. Contrib. Mineral. Petrol. 177, 1–18.
Brune, S., Williams, S.E., Müller, R.D., 2017. Potential links between continental rifting, CO_2 degassing and climate change through time. Nat. Geosci. 10, 941–946.
Canil, D., 1997. Vanadium partitioning and the oxidation state of Archaean komatiite magmas. Nature 389, 842–845.
Catling, D.C., Zahnle, K.J., 2020. The archean atmosphere. Sci. Adv. 6. eaax1420.
Catling, D.C., Zahnle, K.J., McKay, C.P., 2001. Biogenic methane, hydrogen escape, and the irreversible oxidation of early Earth. Science 293, 839–843.
Cottrell, E., Birner, S.K., Brounce, M., Davis, F.A., Waters, L.E., Kelley, K.A., 2021. Oxygen fugacity across tectonic settings. In: Moretti, R., Neuville, D.R. (Eds.), Magma Redox Geochemistry. Wiley, pp. 33–61.

Creech, J., Baker, J., Handler, M., Lorand, J.-P., Storey, M., Wainwright, A., Luguet, A., Moynier, F., Bizzarro, M., 2017. Late accretion history of the terrestrial planets inferred from platinum stable isotopes. Geochem. Perspect. Lett. 3 (1).
Dasgupta, R., Hirschmann, M.M., 2010. The deep carbon cycle and melting in Earth's interior. Earth Planet. Sci. Lett. 298, 1–13.
Delano, J.W., 2001. Redox history of the Earth's interior since ~3900 Ma: implications for prebiotic molecules. Orig. Life Evol. Biosph. 31, 311–341.
Deng, J., Du, Z.X., Karki, B.B., Ghosh, D.B., Lee, K.K.M., 2020. A magma ocean origin to divergent redox evolutions of rocky planetary bodies and early atmospheres. Nat. Commun. 11.
Evans, K.A., 2012. The redox budget of subduction zones. Earth-Sci. Rev. 113, 11–32.
Fischer-Gödde, M., Elfers, B.-M., Münker, C., Szilas, K., Maier, W.D., Messling, N., Morishita, T., Van Kranendonk, M., Smithies, H., 2020. Ruthenium isotope vestige of Earth's pre-late-veneer mantle preserved in Archaean rocks. Nature 579, 240–244.
Frost, D.J., Liebske, C., Langenhorst, F., McCammon, C.A., Tronnes, R.G., Rubie, D.C., 2004. Experimental evidence for the existence of iron-rich metal in the Earth's lower mantle. Nature 428, 409–412.
Frost, D.J., McCammon, C.A., 2008. The redox state of Earth's mantle. Annu. Rev. Earth Planet. Sci. 36, 389–420.
Gaetani, G.A., 2016. The behavior of $Fe^{3+}/\Sigma Fe$ during partial melting of spinel lherzolite. Geochim. Cosmochim. Acta 185, 64–77.
Gaillard, F., Bernadou, F., Roskosz, M., Bouhifd, M.A., Marrocchi, Y., Iacono-Marziano, G., Moreira, M., Scaillet, B., Rogerie, G., 2022. Redox controls during magma ocean degassing. Earth Planet. Sci. Lett. 577, 117255.
Gaillard, F., Scaillet, B., Arndt, N.T., 2011. Atmospheric oxygenation caused by a change in volcanic degassing pressure. Nature 478, 229–232.
Gaillard, F., Scaillet, B., Pichavant, M., Iacono-Marziano, G., 2015. The redox geodynamics linking basalts and their mantle sources through space and time. Chem. Geol. 418, 217–233.
Hamano, K., Abe, Y., Genda, H., 2013. Emergence of two types of terrestrial planet on solidification of magma ocean. Nature 497, 607–611.
Hartley, M.E., Shorttle, O., Maclennan, J., Moussallam, Y., Edmonds, M., 2017. Olivine-hosted melt inclusions as an archive of redox heterogeneity in magmatic systems. Earth Planet. Sci. Lett. 479, 192–205.
Hauri, E.H., Cottrell, E., Kelley, K.A., Tucker, J.M., Shimizu, K., Le Voyer, M., Marske, J., Saal, A.E., 2019. Carbon in the convecting mantle. In: Earth's Deep Carbon: Past to Present. Cambridge University Press.
Hayes, J.M., Waldbauer, J.R., 2006. The carbon cycle and associated redox processes through time. Philos. Trans. R. Soc. Lond. B, Biol. Sci. 361, 931–950.
Herzberg, C., Condie, K., Korenaga, J., 2010. Thermal history of the Earth and its petrological expression. Earth Planet. Sci. Lett. 292, 79–88.
Hirschmann, M.M., 2010. Partial melt in the oceanic low velocity zone. Phys. Earth Planet. Inter. 179, 60–71.
Hirschmann, M.M., 2012. Magma ocean influence on early atmosphere mass and composition. Earth Planet. Sci. Lett. 341, 48–57.
Hirschmann, M.M., 2018. Comparative deep Earth volatile cycles: the case for C recycling from exosphere/mantle fractionation of major (H_2O, C, N) volatiles and from H_2O/Ce, CO_2/Ba, and CO_2/Nb exosphere ratios. Earth Planet. Sci. Lett. 502, 262–273.
Hirschmann, M.M., 2022. Magma oceans, iron and chromium redox, and the origin of comparatively oxidized planetary mantles. Geochim. Cosmochim. Acta 328, 221–241.
Hirschmann, M.M., Dasgupta, R., 2009. The H/C ratios of Earth's near-surface and deep reservoirs, and consequences for deep Earth volatile cycles. Chem. Geol. 262, 4–16.
Holland, H.D., 2002. Volcanic gases, black smokers, and the Great Oxidation Event. Geochim. Cosmochim. Acta 66, 3811–3826.
Hopp, T., Budde, G., Kleine, T., 2020. Heterogeneous accretion of Earth inferred from Mo-Ru isotope systematics. Earth Planet. Sci. Lett. 534.
Huang, R., Ballaran, T.B., McCammon, C.A., Miyajima, N., Dolejš, D., Frost, D.J., 2021. The composition and redox state of bridgmanite in the lower mantle as a function of oxygen fugacity. Geochim. Cosmochim. Acta 303, 110–136.
Hyung, E., Jacobsen, S.B., 2020. The 142Nd/144Nd variations in mantle-derived rocks provide constraints on the stirring rate of the mantle from the Hadean to the present. Proc. Natl. Acad. Sci. 117, 14738–14744.
Itcovitz, J.P., Rae, A.S., Citron, R.I., Stewart, S.T., Sinclair, C.A., Rimmer, P.B., Shorttle, O., 2022. Reduced atmospheres of post-impact worlds: the early Earth. Planetary Sci. J. 3, 115.
Jacobson, S.A., Morbidelli, A., Raymond, S.N., O'Brien, D.P., Walsh, K.J., Rubie, D.C., 2014. Highly siderophile elements in Earth's mantle as a clock for the Moon-forming impact. Nature 508, 84–87.
Jennings, E.S., Holland, T.J., 2015. A simple thermodynamic model for melting of peridotite in the system NCFMASOCr. J. Petrol. 56, 869–892.
Johnson, J.E., Molnar, P.H., 2019. Widespread and persistent deposition of iron formations for two billion years. Geophys. Res. Lett. 46, 3327–3339.
Kadoya, S., Catling, D.C., Nicklas, R.W., Puchtel, I.S., Anbar, A.D., 2020. Mantle data imply a decline of oxidizable volcanic gases could have triggered the Great Oxidation. Nat. Commun. 11, 1–9.
Kasting, J.F., 2013. What caused the rise of atmospheric O2? Chem. Geol. 362, 13–25.
Kasting, J.F., Eggler, D.H., Raeburn, S.P., 1993. Mantle redox evolution and the oxidation state of the Archean atmosphere. J. Geol. 101, 245–257.
King, S.D., Adam, C., 2014. Hotspot swells revisited. Phys. Earth Planet. Inter. 235, 66–83.
Korenaga, J., Planavsky, N.J., Evans, D.A., 2017. Global water cycle and the coevolution of the Earth's interior and surface environment. Philos. Trans. R. Soc. Lond. A, Math. Phys. Eng. Sci. 375, 20150393.
Kump, L.R., Barley, M.E., 2007. Increased subaerial volcanism and the rise of atmospheric oxygen 2.5 billion years ago. Nature 448, 1033–1036.
Kump, L.R., Kasting, J.F., Barley, M.E., 2001. Rise of atmospheric oxygen and the "upside-down" Archean mantle. Geochem. Geophys. Geosyst. 2.
Kuwahara, H., Nakada, R., Kadoya, S., Yoshino, T., Irifune, T., 2023. Hadean mantle oxidation inferred from melting of peridotite under lower-mantle conditions. Nat. Geosci., 1–5.
Laubier, M., Grove, T.L., Langmuir, C.H., 2014. Trace element mineral/melt partitioning for basaltic and basaltic andesitic melts: an experimental and laser ICP-MS study with application to the oxidation state of mantle source regions. Earth Planet. Sci. Lett. 392, 265–278.
Lecuyer, C., Ricard, Y., 1999. Long-term fluxes and budget of ferric iron: implication for the redox states of the Earth's mantle and atmosphere. Earth Planet. Sci. Lett. 165, 197–211.
Lipman, P.W., Calvert, A.T., 2013. Modeling volcano growth on the Island of Hawaii: deep-water perspectives. Geosphere 9, 1348–1383.
Luth, R.W., Stachel, T., 2014. The buffering capacity of lithospheric mantle: implications for diamond formation. Contrib. Mineral. Petrol. 168, 1–12.
Lyons, T.W., Reinhard, C.T., Planavsky, N.J., 2014. The rise of oxygen in Earth's early ocean and atmosphere. Nature 506, 307–315.
Maier, W.D., Barnes, S.J., Campbell, I.H., Fiorentini, M.L., Peltonen, P., Barnes, S.-J., Smithies, R.H., 2009. Progressive mixing of meteoritic veneer into the early Earth's deep mantle. Nature 460, 620–623.
Marty, B., Tolstikhin, I.N., 1998. CO_2 fluxes from mid-ocean ridges, arcs and plumes. Chem. Geol. 145, 233–248.
Maurice, M., Dasgupta, R., Hassanzadeh, P., 2023. Redox evolution of the crystallizing terrestrial magma ocean and its influence on the outgassed atmosphere. Planetary Sci. J. 4, 31.
McKenzie, D., 2020. Speculations on the generation and movement of komatiites. J. Petrol. 61, egaa061.
Miller, S.L., Urey, H.C., 1959. Organic compound synthesis on the primitive Earth: several questions about the origin of life have been answered, but much remains to be studied. Science 130, 245–251.
Moussallam, Y., Longpre, M.-A., McCammon, C., Gomez-Ulla, A., Rose-Koga, E.F., Scaillet, B., Peters, N., Gennaro, E., Paris, R., Oppenheimer, C., 2019. Mantle plumes are oxidised. Earth Planet. Sci. Lett. 527.
Nicklas, R.W., I.S., P., 2019, Ash, R.D., Piccoli, H.M., Hanski, E., Nisbet, E.G., Waterton, P., Pearson, D.G., Anbar, A.D. Secular mantle oxidation across the Archean-Proterozoic boundary: evidence from V partitioning in komatiites and picrites. Geochim. Cosmochim. Acta 250, 49–75.
Nicklas, R.W., Puchtel, I.S., Ash, R.D., 2018. Redox state of the Archean mantle: evidence from V partitioning in 3.5–2.4 Ga komatiites. Geochim. Cosmochim. Acta 222, 447–466.
O'Neill, H.S.C., Rubie, D., Canil, D., Geiger, C., Ross, C., Seifert, F., Woodland, A., 1993. Ferric iron in the upper mantle and in transition zone assemblages: implications for relative oxygen fugacities in the mantle. Geophys. Monogr. 74, 73–88.
O'Neill, C., Aulbach, S., 2022. Destabilization of deep oxidized mantle drove the Great Oxidation Event. Sci. Adv. 8, eabg1626.
Pahlevan, K., Schaefer, L., Hirschmann, M.M., 2019. Hydrogen isotopic evidence for early oxidation of silicate Earth. Earth Planet. Sci. Lett. 526.
Parkinson, I.J., Arculus, R.J., 1999. The redox state of subduction zones: insights from arc-peridotites. Chem. Geol. 160, 409–423.
Rosenthal, A., Hauri, E.H., Hirschmann, M., 2015. Experimental determination of C, F, and H partitioning between mantle minerals and carbonated basalt, CO_2/Ba and CO_2/Nb systematics of partial melting, and the CO_2 contents of basaltic source regions. Earth Planet. Sci. Lett. 412, 77–87.
Scaillet, B., Gaillard, F., 2011. Redox state of early magmas. Nature 480, 48–49.
Schaefer, L., Fegley, B., 2010. Chemistry of atmospheres formed during accretion of the Earth and other terrestrial planets. Icarus 208, 438–448.
Schlichting, H.E., Sari, R.e., Yalinewich, A., 2015. Atmospheric mass loss during planet formation: the importance of planetesimal impacts. Icarus 247, 81–94.
Sinclair, C.A., Wyatt, M.C., Morbidelli, A., Nesvorný, D., 2020. Evolution of the Earth's atmosphere during Late Veneer accretion. Mon. Not. R. Astron. Soc. 499, 5334–5362.
Sleep, N.H., Zahnle, K., 2001. Carbon dioxide cycling and implications for climate on ancient Earth. J. Geophys. Res., Planets 106, 1373–1399.
Sossi, P.A., Burnham, A.D., Badro, J., Lanzirotti, A., Newville, M., O'Neill, H.S., 2020. Redox state of Earth's magma ocean and its Venus-like early atmosphere. Sci. Adv. 6.
Stagno, V., Aulbach, S., 2022. Redox processes before, during, and after Earth's accretion affecting the deep carbon cycle. In: Moretti, R., Neuville, D.R. (Eds.), Magma Redox Geochemistry. Wiley, pp. 19–32.
Stagno, V., Ojwang, D.O., McCammon, C.A., Frost, D.J., 2013. The oxidation state of the mantle and the extraction of carbon from Earth's interior. Nature 493 84-+.

Stolper, D.A., Higgins, J.A., Derry, L.A., 2021. The role of the solid earth in regulating atmospheric O_2 levels. Am. J. Sci. 321, 1381–1444.
Stolper, D.A., Keller, C.B., 2018. A record of deep-ocean dissolved O_2 from the oxidation state of iron in submarine basalts. Nature 553, 323–327.
Stolper, E.M., Shorttle, O., Antoshechkina, P.M., Asimow, P.D., 2020. The effects of solid-solid phase equilibria on the oxygen fugacity of the upper mantle. Am. Mineral.: J. Earth Planet. Mat. 105, 1445–1471.
Taracsák, Z., Hartley, M., Burgess, R., Edmonds, M., Iddon, F., Longpré, M., 2019. High fluxes of deep volatiles from ocean island volcanoes: insights from El Hierro, Canary Islands. Geochim. Cosmochim. Acta 258, 19–36.
Thompson, K.J., Kenward, P.A., Bauer, K.W., Warchola, T., Gauger, T., Martinez, R., Simister, R.L., Michiels, C.C., Llirós, M., Reinhard, C.T., 2019. Photoferrotrophy, deposition of banded iron formations, and methane production in Archean oceans. Sci. Adv. 5. eaav2869.
Trail, D., Watson, E.B., Tailby, N.D., 2011. The oxidation state of Hadean magmas and implications for early Earth's atmosphere. Nature 480, 79-U238.
Tucker, J.M., Hauri, E.H., Pietruszka, A.J., Garcia, M.O., Marske, J.P., Trusdell, F.A., 2019. A high carbon content of the Hawaiian mantle from olivine-hosted melt inclusions. Geochim. Cosmochim. Acta 254, 156–172.
Walker, J., 1977. Evolution of the Atmosphere. Macmillan Publ., NY.
Wong, K., Mason, E., Brune, S., East, M., Edmonds, M., Zahirovic, S., 2019. Deep carbon cycling over the past 200 million years: a review of fluxes in different tectonic settings. Front. Earth Sci. 7, 263.
Wood, B.J., Virgo, D., 1989. Upper mantle oxidation-state - ferric iron contents of lherzolite spinels by Fe-57 Mössbauer-spectroscopy and resultant oxygen fugacities. Geochim. Cosmochim. Acta 53, 1277–1291.
Zahnle, K.J., Gacesa, M., Catling, D.C., 2019. Strange messenger: a new history of hydrogen on Earth, as told by Xenon. Geochim. Cosmochim. Acta 244, 56–85.
Zahnle, K.J., Lupu, R., Catling, D.C., Wogan, N., 2020. Creation and evolution of impact-generated reduced atmospheres of early Earth. Planetary Sci. J. 1, 11.
Zhang, H.L., Cottrell, E., Solheid, P.A., Kelley, K.A., Hirschmann, M.M., 2018. Determination of $Fe^{3+}/\Sigma Fe$ of XANES basaltic glass standards by Mössbauer spectroscopy and its application to the oxidation state of iron in MORB. Chem. Geol. 479, 166–175.
Zhang, Z., Qin, T., Pommier, A., Hirschmann, M.M., 2019. Carbon storage in Fe-Ni-S liquids in the deep upper mantle and its relation to diamond and Fe-Ni alloy precipitation. Earth Planet. Sci. Lett. 520, 164–174.